ACS Sustainable Chemistry & Engineering

pubs.acs.org/journal/ascecg

Research Article

Chiral Self-Assembly Behavior of Carboxylated Cellulose Nanocrystals Isolated by Recyclable Oxalic Acid from Degreasing Cotton

Chunxiang Lin, Ping Wang, Yifan Liu, Yuancai Lv, Xiaoxia Ye, Minghua Liu,* and J. Y. Zhu*

Cite This: ACS Sustainable Chem. Eng. 2023, 11, 8035−8043

Read Online

ACCESS | Metrics & More | Article Recommendations | Supporting Information

ABSTRACT: Carboxylated cellulose nanocrystals (OA-CNCs) isolated by aqueous recyclable oxalic acid hydrolysis from degreasing cotton were used to observe its self-assembly behavior and chiral nematic properties. The oxalic acid here served as the sole catalyst to esterify and hydrolyze the degreasing cotton. The results indicated that the obtained OA-CNC suspensions were spontaneously phase-separated into a chiral nematic mesophase above a critical concentration, and the occurrence of chiral self-assembly is highly dependent on the aspect ratio and the surface charge of the OA-CNC suspension. Scanning electron microscopy images of the cross section of OA-CNC solid films revealed a periodic ordered multilayer structure. The residual OA was easily recovered through simple re-crystallization method after reactions with a high recovery rate of at least 90%. The recycled OA (ROA) had excellent performance in terms of ROA-CNC yield even after reusing for five cycles. Moreover, the resultant ROA-CNCs from recycled OA could also form chiral nematic ordered phases with little change in the critical concentration and pitch, suggesting excellent suitability for sustainable OA-CNC production for photonics and other specialty applications.

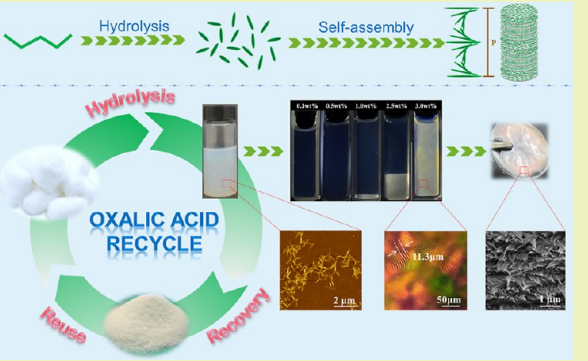

KEYWORDS: *carboxylated cellulose nanocrystals, recyclable oxalic acid, chiral nematic liquid crystal, self-assembly, sustainable production*

INTRODUCTION

Cellulose nanocrystals (CNCs), a biosourced nanomaterial produced from cellulose, have gained increasing attention in recent decade due to its particular physicochemical properties.[1−3] A fascinating characteristic of the CNCs is that it can form a chiral nematic (also called cholesteric) lyotropic liquid crystal phase spontaneously above a critical concentration in water,[4,5] making it a valuable material applied in sensing, anticounterfeiting, or decoration.[6]

Generally, colloidal stability of CNC aqueous systems is a precondition that directly determines whether the self-assembly of CNCs can take place.[4] CNCs produced by concentrated sulfuric acid hydrolysis (S−CNCs) can easily form a chiral nematic lyotropic liquid crystal phase[7] because they have a negative charge due to the presence of half-ester sulfate groups on the surface that imparts S−CNCs excellent colloidal stability, thus forming highly stable dispersion system through strong electrostatic repulsion.[8] When the concentration of the stable colloidal suspension is above a critical value, the chiral nematic liquid crystal phase is generated by self-assembly.[9] Therefore, S−CNCs have been almost exclusively used in studying the chiral nematic properties of CNCs for promising applications. However, S−CNCs facing production and environmental challenges due to difficulties in economic acid recovery, the need for disposal of salts from acid neutralization, and the strong corrosivity of sulfuric acid.

Carboxylated CNCs prepared through TEMPO-mediated oxidation of S−CNCs (T-S-CNCs) were found to have liquid crystal properties.[10] The introduction of carboxyl groups through TEMPO oxidation also produced electrostatic repulsion between CNC particles and form the stable colloidal suspension. However, TEMPO S−CNCs suffers the same production and environmental issues as those for producing S−CNCs in addition to the cost for TEMPO and extra processing steps.[11] Other CNC production methods including ammonium persulfate (APS) oxidation,[12] periodate-chlorite oxidation,[13] $KMnO_4$ oxidation,[14] citric/hydrochloric acid hydrolysis,[15] and alkaline periodate oxidation[16,17] have been developed to improve sustainability in CNC production. However, these methods are challenged by some concerns,

Received: January 7, 2023
Revised: April 27, 2023
Published: May 15, 2023

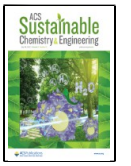

https://doi.org/10.1021/acssuschemeng.3c00118
ACS Sustainable Chem. Eng. 2023, 11, 8035−8043

Table 1. Characteristics of Cotton and OA-CNC Samples

		OA-CNC properties						self-assembly behavior		
cellulose sample	yield (%)	aspect ratio[a]	height range[b] (nm)	carboxyl content (mmol/g)	surface charge[c] (mV)	CrI (%)	DP	$*C_1$[d]	$*C_2$[e]	pitch (μm)
degreasing cotton	-	-	-	-	-	74.5	582	-	-	-
O(60, 100, 3)	14.74	5.1	4−24	0.12	−25.28	78.7	282			
O(60, 105, 3)	16.81	5.2	3−20	0.13	−27.88	79.3	277			
O(70, 105, 3)	15.07	6.6	5−23	0.13	−30.24	82.9	264	1.33	3.08	10.5
O(80, 105, 3)	24.38	6.8	4−19	0.16	−35.74	85.5	235	0.74	2.99	11.3
O(80, 100, 3)	21.98	6.2	4−29	0.11	−33.02	84.8	234	1.52	3.29	9.8
O(80, 110, 3)	27.23	5.6	8−34	0.17	−35.37	86.4	219	0.99	3.84	12.7
O(80, 105, 2)	18.2	6.4	3−21	0.12	−28.19	82.2	227	1.06	3.20	10.1
O(80, 105, 4)	33.36	7.3	4−23	0.11	−35.55	85.7	208	0.91	3.11	9.9
O(80, 100, 4)	23.15	7.9	5−12	0.17	−36.28	84.1	223	0.69	2.79	14.4
S(64,45,1)	17.92	9.7	4−27		−45.67	89.0	183	6.44	7.94	7.2

[a]Taken as the ratio length/width. [b]Obtained from AFM measurement. [c]Measured by ζ potential. [d]$*C_1$, first critical concentration at which tactoids were formed in the CNC suspension, wt %. [e]$*C_2$, second critical concentration at which the CNC suspension became fully anisotropic, wt %.

such as high chemical cost, large energy consumption, and poor reagent recyclability and reusability.

Solid organic acids have attracted interest for producing CNCs for its low corrosivity and ease in recycling,[18,19] especially the dicarboxylic acids, which could achieve satisfactory aqueous dispersibility of CNCs ascribed to the presence of surface carboxyl groups,[20] providing the possibility for the self-assembly of CNC suspension. Lately, we successfully prepared carboxylated CNCs (DC-CNCs) from cotton linter by dicarboxylic acid hydrolysis. The resultant DC-CNCs were able to self-assemble with liquid crystal properties,[21] especially with the application of a catalyst and/or an organic solvent. However, additional processing costs will incur especially using organic solvents. Compared with maleic acid and succinic acid used in our earlier study,[21] oxalic acid (OA) has higher acidity (pKa_1 = 1.23) and is more effective in CNC isolation and carboxylation,[22] CNCs with 0.3−1.2 mmol/g carboxyl group content was reported.[19] Moreover, CNC suspension obtained by molten OA dehydrate hydrolysis could present birefringence patterns.[23] However, few studies focused on the chiral nematic liquid crystal behavior of carboxylated CNCs isolated by aqueous OA hydrolysis (OA-CNCs) without the application of organic solvent and catalysts. The objective of the present study is to demonstrate the self-assembly behavior of OA-CNCs derived from aqueous OA hydrolysis along with the recyclability of oxalic acid and the efficacy of the recycled OA. The goal of the study is to achieve sustainable production of OA-CNCs with chiral nematic liquid properties for advanced CNC applications such as in photonics and light management.

EXPERIMENTAL SECTION

Materials. Degreasing cotton, obtained from Yanggu Jingyanggang Sanitary Materials Factory, was crushed to 20−50 μm and then dried before use. Oxalic acid (OA, 99.5%) was purchased from Sinopharm, Chemical Reagent Co., Ltd. All other reagents were of analytical grade and purchased from Aladdin (China).

Preparation of OA-CNCs. CNCs were isolated by heating a mixture of 100g 60−80 wt % OA and degreasing cotton (3 g) in an oil bath at 100−110 °C for 2 to 4 h. At the end of the reaction, about 200 mL warm water was added to quench the reaction. The obtained mixture was then filtered immediately to separate the solids from the unreacted OA solution. The filtrate was then crystallized for later reuse. The solids were washed with water and then centrifuged repeatedly until the supernatant was turbid. The turbid supernatant was collected and dialyzed using a dialysis bag until the conductivity of the dialysis water no longer changed. Yield of the resultant OA-CNCs was calculated by dividing the mass of OA-CNCs by the mass of the original degreasing cotton. As a control, sample of CNCs isolated by sulfuric acid hydrolysis was obtained by treating degreasing cotton with 64% of sulfuric acid at 45 °C for 1 h, and the sample was denoted as S−CNCs.

OA-CNC films were obtained by the conventional solution casting method:[24] 8 mL of 2 wt % OA-CNC suspension was processed with sonication for about 10 min through an ultrasonic processor (KQ5200DE, Ultrasonic Equipment Co., Ltd., Shanghai, China). The treated suspension was then immediately poured into a plastic dish (35 mm in diameter). The suspension was left undisturbed and slowly evaporated under ambient conditions to obtain a solid film.

OA Recycling and Reuse. The collected supernatant (diluted hydrolysate) was cooled to 4 °C for crystallization. The obtained crystals were separated followed by dissolution in warm water and then re-crystallized again. To evaluate the efficacy of the recycled OA, the recycled OA was reused to hydrolyze fresh degreasing cotton.

Characterization. Fourier transform infrared (FTIR) spectra of samples were measured on a spectrometer (Nicolet is5, Nicolet, USA) with a range from 500 to 4000 cm^{-1}. The X-ray diffraction (XRD) patterns were measured using an X-ray diffractometer (MiniFlex 600, Rigaku, Tokyo, Japan) equipped with copper radiation (λ = 0.154 nm). The crystallinity index (CrI) of a cellulose sample was calculated according to the Segal method[25] with baseline subtraction

$$\text{CrI}\ (\%) = \frac{I_{002} - I_{am}}{I_{002}} \times 100\% \quad (1)$$

where I_{002} corresponds to the maximum diffraction intensity of the 002 lattice and I_{am} corresponds to the intensity at 2θ = 18°.

Surface compositions of the OA-CNCs were evaluated by X-ray photoelectron spectroscopy (XPS, ESCALAB 250, Thermo Fisher Scientific). The transmittance of films was scanned on an R1 angle-resolved spectroscopy system (Idea Optics) in the wavelengths ranging from 500 to 4000 nm.

Topographical images of OA-CNC samples were obtained by atomic force microscopy (AFM) (5500, Agilent Technologies, Folsom, California, USA) in the tapping mode. The morphology of OA-CNCs (a suspension of 0.05 wt ‰ placed on a copper grid, negatively stained with 2% uranyl acetate) were analyzed using Tecnai G2F20 scanning transmission electron microscope. The cross-sectional morphology of the OA-CNC film was obtained by a scanning electron microscope (Verios G4 UC, FEI Company, Hillsboro, Oregon, USA). Before observation, samples were embrittled with liquid nitrogen, spraying gold for 45 s.

The optical characteristics of OA-CNC suspension and solid films were determined on a polarized optical microscope (ZYP-1000E POM, Zhongnuo, China). The photographs of the films were taken

https://doi.org/10.1021/acssuschemeng.3c00118
ACS Sustainable Chem. Eng. 2023, 11, 8035−8043

by a smartphone camera. Circularly polarized luminescence (CPL) spectrum of OA-CNC films was recorded using a JASCO CPL-300 spectrophotometer and the corresponding luminescence dissymmetry factors (g_{lum}) were reported by the spectrophotometer.

Other experimental protocols and instrumentation, including liquid chromatography, ζ potential measurement, and carboxyl group content are described in the Supporting Information.

RESULTS AND DISCUSSION

OA-CNC Yield and Properties. As reported earlier,[19,22] a significant amount of cellulose will remain in the form of fibers and OA-CNC yield is lower after concentrated OA hydrolysis even under elevated temperatures because OA is a weak acid. As listed in Table 1, OA-CNC yield varied from approximately

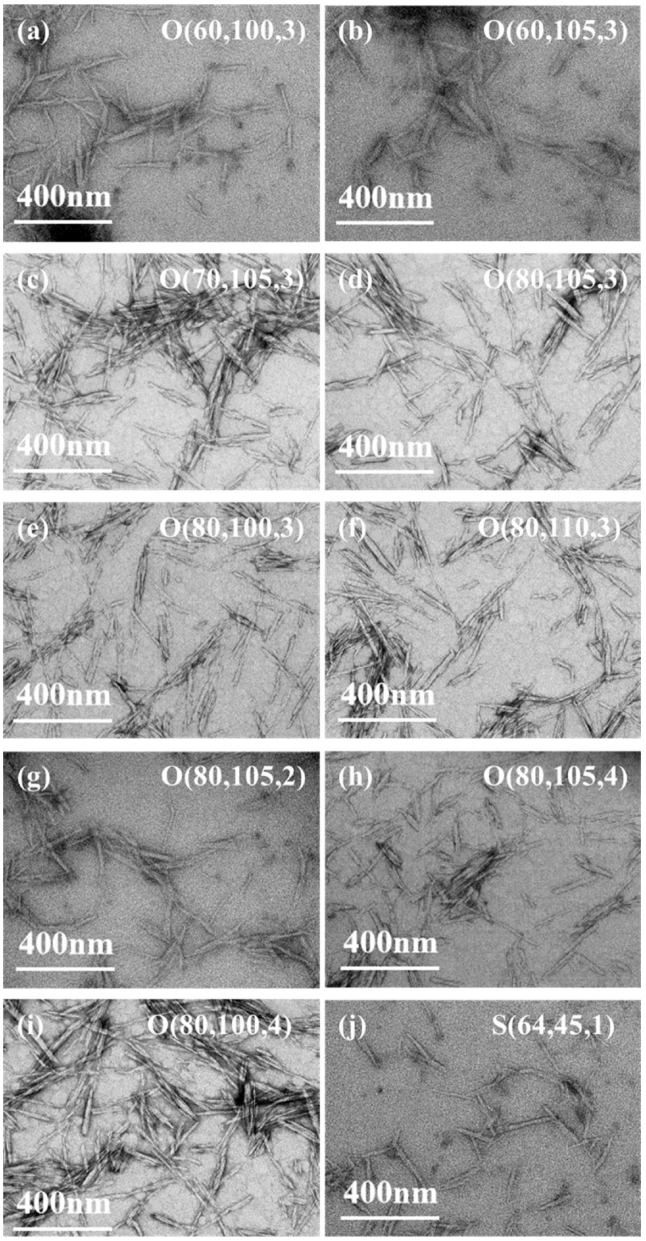

Figure 1. TEM images (a–j) of CNC samples extracted under different conditions. (a) O(60, 100, 3); (b) O(60, 105, 3); (c) O(70, 105, 3); (d) O(80, 105, 3); (e) O(80, 100, 3); (f) O(80, 110, 3); (g) O(80, 105, 2); (h) O(80, 105, 4); (i) O(80, 100, 4); and (j) S(64, 45, 1).

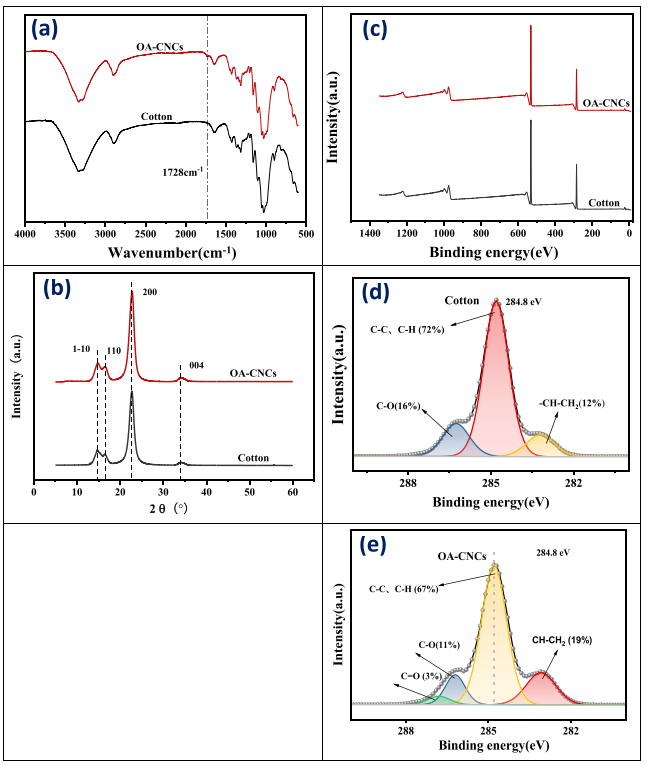

Figure 2. (a) FTIR, (b) XRD, and (c) XPS spectra. (d,e) Deconvolutions of the C1 peaks of cotton and O(80, 105, 3) samples.

15% to over 30% for the range of hydrolysis conditions carried out. This is in agreement with an earlier study.[19] To facilitate discussion, the obtained CNC samples are labeled using abbreviated hydrolysis conditions as A(*xx*, *yyy*, *z*) to represent acid A (O for oxalic acid and S for sulfuric acid) at an acid concentration of *xx* wt %, reaction temperature *yyy* °C, for a reaction duration of *z* h. The data in Table 1 show that increasing acid loading and hydrolysis time or reaction temperature increased CNC yield. The highest yield of 33.36% was obtained under the conditions of 80 wt % acid concentration and 105 °C for 4 h, severer than that for S(64, 45, 1). TEM (Figure 1) and AFM (Figure S1) images of the OA-CNCs illustrate that the nanoparticles were polydisperse in physical dimensions. Length and width distributions (Figure S2) along with the height measured by AFM (Table 1) of OA-CNCs demonstrate that the shape of particles were flat objects, similar to those obtained by the sulfuric acid method.[26] The average thickness of OA-CNC particles was around 15 nm for an average width about 100 nm and a length ranging from 200 to 1000 nm. Aspect ratios of OA-CNC ranged from 5.1 to 7.9 and seemed to increase with the increasing acid concentration or hydrolysis time. The surface charge and carboxyl group content of the OA-CNCs ranged from −25 to −37 mV and from 0.11 to 0.17 mmol/g, respectively, implying that well dispersion of the colloidal suspensions can be achieved. Increasing hydrolysis temperature also promoted cellulose esterification (or carboxylation). The stability of the colloidal suspension dictated the formation of the lyotropic liquid crystal phase. In comparison, the CNCs resulted from sulfuric acid hydrolysis of degreasing cotton [S(64, 45, 1)] (Figure 1j) S−CNCs have smaller dimensions, a larger aspect ratio and higher surface charge, thus making it easier to form chiral nematic liquid crystal.

https://doi.org/10.1021/acssuschemeng.3c00118
ACS Sustainable Chem. Eng. 2023, 11, 8035−8043

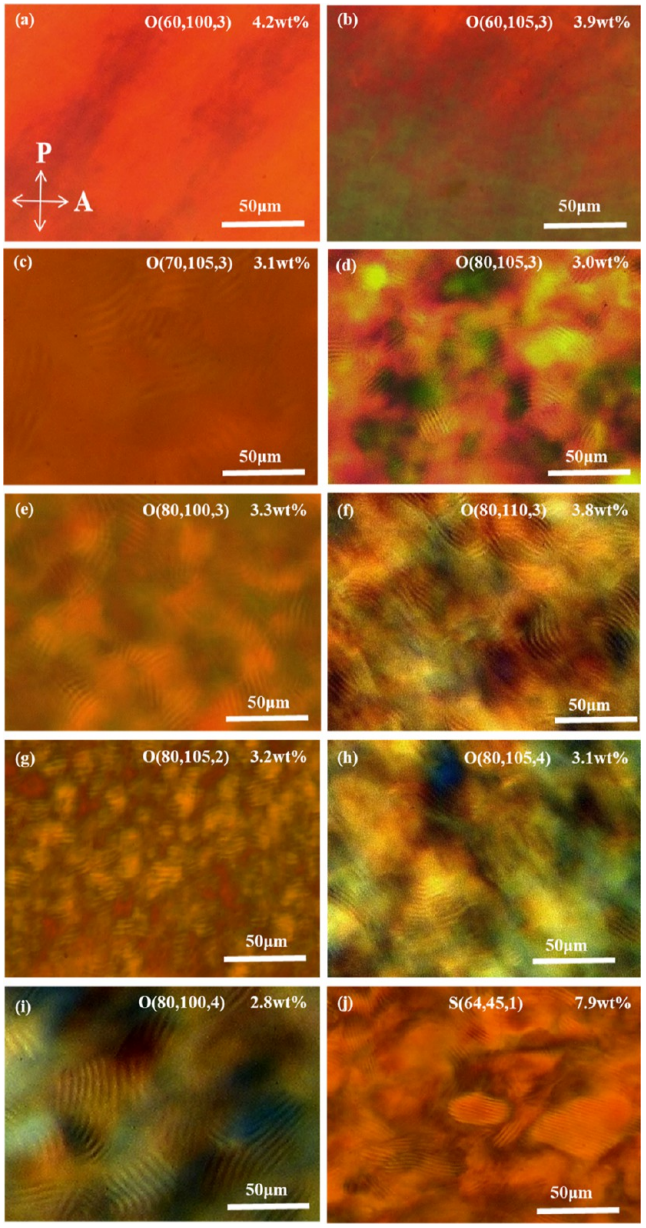

Figure 3. POM images (a–j) of CNC samples extracted under different conditions [arrows indicating directions of the polarizer (P) and analyzer (A); samples were sandwiched between P and A].

The chemical structure of OA-CNCs was characterized by FTIR, XRD, and XPS. Comparisons of FTIR spectra between the degreasing cotton and OA-CNCs can show the changes in chemical structure through OA hydrolysis. OA-CNCs show a new peak at 1725 cm^{-1}, corresponding to C═O stretching, indicating the presence of the carboxyl group on the OA-CNC surface due to cellulose esterification (Figure 2a). XRD results exhibited the typical cellulose I_β diffraction peaks at about 2θ = 14.6, 16.4, 22.8, and 34.2° assigned to the (−110), (110), (200), and (004) reflection planes, respectively (Figure 2b). Compared with original degreasing cotton, OA-CNCs showed a more intensive peak at 22.8° because of the enhancement of crystallinity due to the removal of disordered cellulose by OA hydrolysis, and all the CNC samples had a higher CrI (Table 1) due to hydrolysis of disordered cellulose. The average DP values of the degreasing cotton and CNC samples were tested and are listed in Table 1. The DP value of degreasing cotton exhibited a significant decrease from 582 to 282−183 after hydrolysis, suggesting that the molecular chains of cellulose were fragmented in the amorphous region at certain intervals, as reported by Sun et al.[27]

The existence of carboxyl groups was also verified by XPS. Two peaks at 533 and 285 eV, which was assigned to oxygen and carbon, respectively, were observed in both XPS spectra (Figure 2c). The C1s peak were fitted with four components, including peaks around 284.6, 286.3, 288.0, and 289.0 eV assigned to C1 (C−C/C−H), C2 (C−O), C3 (O−C−O and/or C═O), and C4 (O−C═O), respectively.[28] Compared with original degreasing cotton (Figure 2d), OA-CNCs exhibited the fourth peak from C4 (Figure 2e), confirming the existence of −COOH on OA-CNCs.

Chiral Self-Assembly Behavior of OA-CNCs. As is well known, suspensions of CNCs from sulfuric acid hydrolysis easily form a chiral nematic liquid crystal phase spontaneously above a critical concentration. The occurrence of such self-assembly highly depends on the CNC properties.[29,30] The aspect ratio and surface charge are the two main characteristics of OA-CNCs that play an important role in their self-assembly behavior.[31,32] Formations of chiral nematic liquid crystal phase for all samples were investigated by POM images as shown in Figure 3. It could be seen that no fingerprint texture was observed in POM images for samples O(60, 100, 3) and O(60, 105, 3) obtained at an OA concentration of 60 wt % even at an OA-CNC suspension concentration above 4% (Figure 3a,b), perhaps, due to the low aspect ratio (Table 1) and low surface charge of these two samples.

Samples with an aspect ratio above 5.5 and surface charge above 30.0 mV were all able to form the chiral liquid crystal phase. The $*C_2$ for the suspension ranged from 2.4−3.0% with pitches between 13 and 20 μm, much lower than that of S−CNCs at approximately 8% with a smaller pitch of 7.2 μm. The data shown in Table 1 also demonstrate that the higher aspect ratios of OA-CNCs lead to lower $*C_2$, which was consistent with Onsager's phase separation theory.[33,34] The above results demonstrate that OA-CNCs have the ability to form the chiral liquid crystal phase, promising for applications in CNC-based chiral composites.

To further investigate the self-assembly behavior of OA-CNCs, the formation process of the chiral nematic liquid crystal phase was recorded. Images of the suspension using sample O(80, 105, 3) with the concentrations of 0.3, 0.5, 0.8, 1.0, 2.5, and 3.0 wt % sandwiched between two crossed polarizers, respectively, are demonstrated in Figure 4a. When the concentration was below 1.0%, the suspension was optically isotropic. The suspension became biphasic with the upper phase optically isotropic and the lower phase optically anisotropic as the concentration was increased to 1.0%. Besides, the fraction of the anisotropic phase increased with the CNC concentration until the suspension became fully anisotropic at 3.0 wt % (Figure 4b). The corresponding characteristic fingerprints of OA-CNCs were also presented through POM images (Figure 4c). It could be seen that the suspension forms tactoids first at a CNC concentration of 0.8 wt %, then fingerprint texture emerged from the occurrence of phase separation with increasing concentration, and finally well-ordered fingerprint texture could be observed when the suspension was completely anisotropic. As is usually observed, the pitch decreases with increasing concentration. However, OA-CNC suspensions would transit to a gel state at a higher initial concentration (>4.0%), where only birefringence but no

https://doi.org/10.1021/acssuschemeng.3c00118
ACS Sustainable Chem. Eng. 2023, 11, 8035−8043

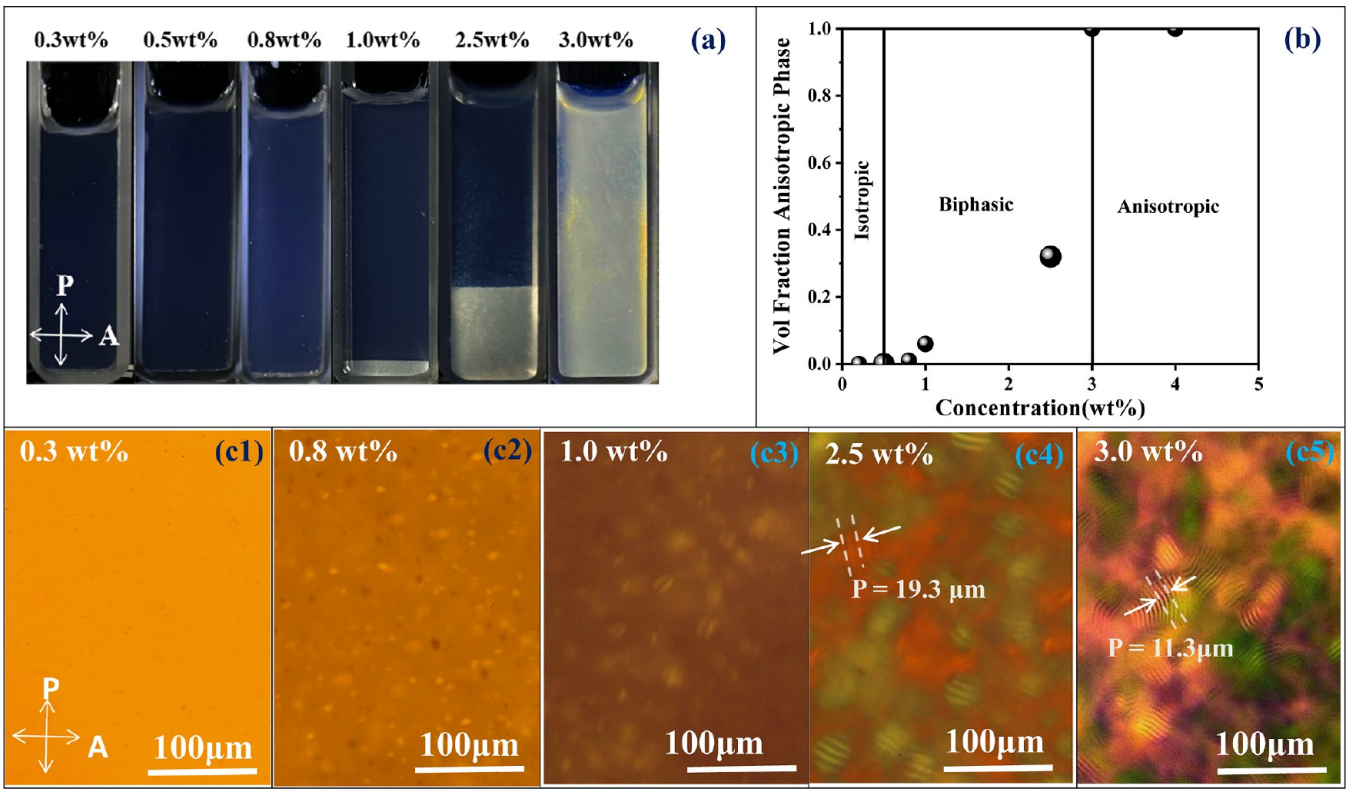

Figure 4. (a) Phase separation observed between cross polars for sample O (80, 105, 3) in different concentrations, (b) corresponding phase transition diagram for O (80, 105, 3), and (c) POM photographs of O (80, 105, 3) suspensions with different concentrations.

chiral ordering was observed (Figure S1). The reason might be due to the restriction of the strong physical cross-linking network of the carboxyl group at higher concentrations.[35]

One of the fascinating characteristics of CNCs is that the chiral nematic structure observed in their suspensions can be preserved in films, greatly expanding their applications.[24,36,37] The OA-CNC films displayed iridescent color (Figure 5a) and fingerprint texture as clearly observed (Figure 5b). Image of cross-sectional morphology of the solid film is also presented (Figure 5c). From the cross-sectional SEM images, a highly ordered layered structure was clearly observed; the enlarged SEM image (Figure 5d) demonstrated that the CNCs were arranged regularly to form a periodic helical structure in the film. The helical pitch was measured to be approximately 4.3 μm, lower than the value obtained by POM.

Additionally, the response to water on the OA-CNC film was evaluated under natural light. As shown in the inset figures in Figure 5e–g, the dried OA-CNC film had a blue color but changed to yellow after wetting. However, the film turned to blue color again after being dried. The change in the pitch before and after wetting is shown in Figure 5e–g. The pitch was about 4.6 μm at its initial dry state and then increased to about 6.8 μm in the wet state, and recovered to 4.3 μm again after re-drying. Based on Bragg's reflection, the increase in pitch leads to increase in λ_{max} of the film (a red shift in the reflectance peak), which can be seen by the color change from blue to yellow with increasing humidity.[38] Reflection spectra of the solid film by UV–vis (Figure 5h) proved the occurrence of red shift in reflectance peak after being wetted by water droplet and then returned to the initial state when re-dried in room temperature. Circularly polarized fluorescence spectrum (CPL) of the OA-CNC film is shown in Figure 5i, in which the film displays positive circular dichroism signals with a g_{lum} value of 0.036, confirming the ability of the OA-CNC film to selectively reflect left-handed circularly polarized light.[39]

Recycle and Reuse of OA. The dicarboxylic acid hydrolysis method[19] for producing CNCs only uses one chemical, which facilitates the recycling of OA for reuse. The recovery and recycle of the unreacted OA after hydrolysis were evaluated. Through OA crystallization from the hydrolysate, the unreacted OA was recovered as shown in Figure 6a. Compared with fresh OA, the recovered OA maintained the crystal-like shape but displayed gradual brown color with the increasingly recycling cycles, most likely from the impurities and degradation byproducts. Liquid chromatographic results (Figure 6b) showed that the hydrolysates mainly contained mannose (7.7%), xylose (5.3%), and glucose (87.0%). Figure 6c,d revealed the high recovery rate and structural stability of the OA after five cycles.

The performance of the recovered OA was evaluated by the yields and dimensions of the CNCs (ROA-CNCs) extracted using recycled OA. As demonstrated in Figure 6c, the yields of ROA-CNCs were slightly decreased from 24.38 to 21.57% after five recycles, and the morphology and size distribution of the ROA-CNCs (Figures 6e–g and S4) were most likely unchanged compared with that of OA-CNCs from using fresh OA. The self-assembly property of the ROA-CNCs was also evaluated. Figures 6h and S5 present the POM images of ROA-CNC suspensions at $*C_2$ critical concentrations with little change in the value of P, indicating that all samples showed fingerprint patterns, conforming the formation of the CNC chiral nematic liquid phase.

Based on the above results, the recovered OA still showed excellent performance after being recycled for at least five

https://doi.org/10.1021/acssuschemeng.3c00118
ACS Sustainable Chem. Eng. 2023, 11, 8035–8043

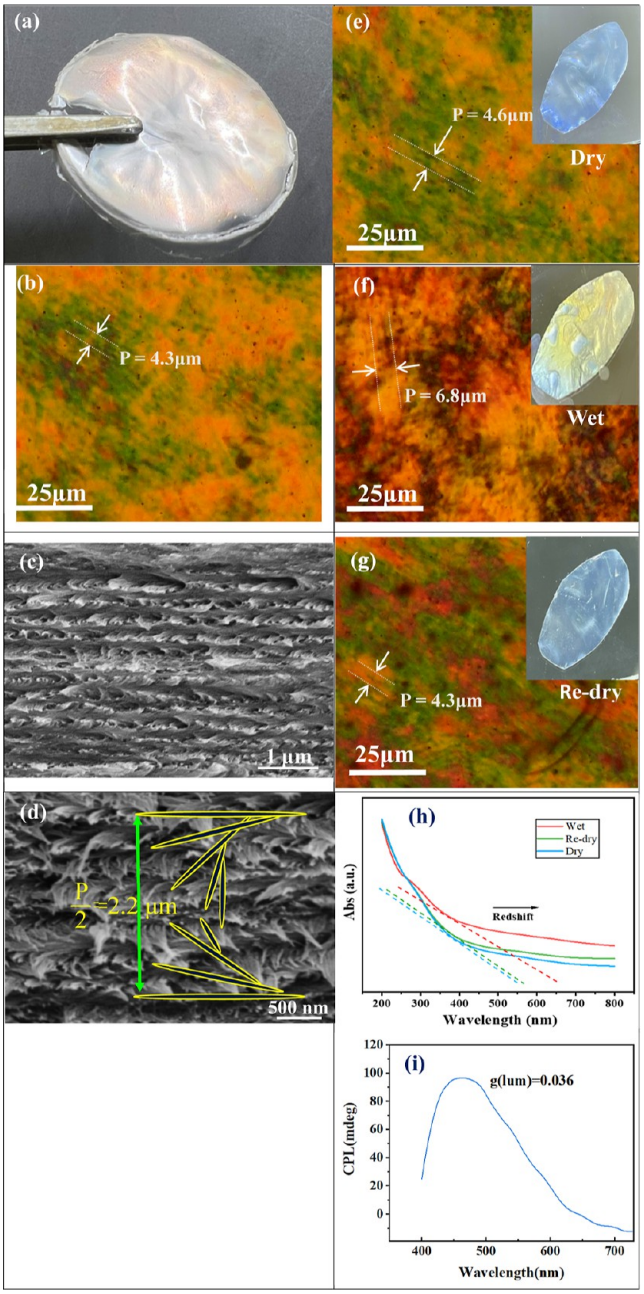

Figure 5. (a) Photo of the film; (b) POM image of the film; (c,d) cross-sectional SEM images of the film; (e–g) POM images of the film in dry, wet, and re-dry states; all insets are photographs of the film in dry and wet states; (h) UV–vis spectrum of the film in dry and wet states; and (i) CPL spectrum of the film.

times, implying its suitability for continuous CNC isolation, providing a promising method for isolating CNCs with self-assembly ability and improved reagent utilization.

Different preparation methods and corresponding performance of self-assembly ability for CNCs are listed in Table 2. Compared with other methods reported in the literature, the method described in this work is simpler and quicker without any other additives or procedure expect for oxalic acid hydrolysis. Moreover, the CNCs obtained by this method could form chiral nematic liquid crystals above a lower critical concentration (1.0%), promoting the market adaption of this renewable nanomaterial. Because of the easy recycle and less environmental impact of OA, the preparation of OA-CNC in

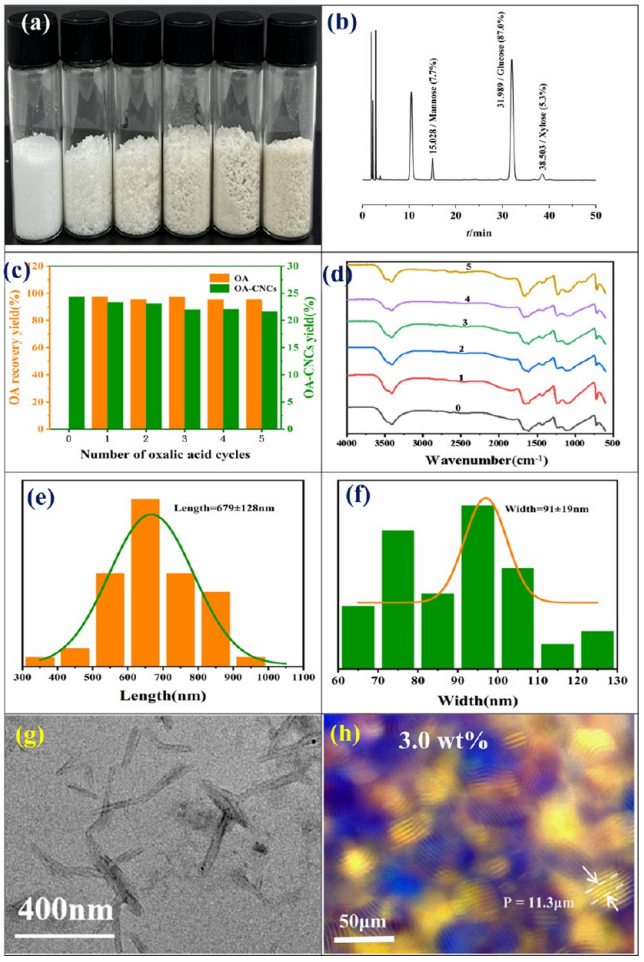

Figure 6. (a) Photo of the recovered OA; (b) liquid chromatogram of hydrolysate; (c) recovery rate of OA and yield of CNCs under different cycles; (d) FTIR spectra of CNCs under different cycles; (e) length and (f) width distribution, and (g) TEM and (h) POM images of the ROA-CNCs obtained using OA recycled five times.

such a manner is expected to facilitate the scaling up of the preparation.

CONCLUSIONS

OA-CNCs with uniform nanoscale morphology were extracted from degreasing cotton through simultaneous esterification and hydrolysis by recyclable oxalic acid. Phase separation of OA-CNC suspensions was detected above a critical concentration and fingerprint texture was observed. The formation of the CNC chiral liquid crystal phase was influenced by the CNC properties with a second critical concentration ranging from 2.4 to 3.0%, much lower than that of CNCs isolated by sulfuric acid hydrolysis. Additionally, the OA-CNC solid film displayed a highly ordered layered structure and sensitive moisture response, implying the good preservation of the chiral nematic structure. The performance of OA was maintained even after five recycles in terms of CNC yield, with no obvious difference observed in morphology and ability in forming the chiral nematic crystal phase.

ASSOCIATED CONTENT

Supporting Information

The Supporting Information is available free of charge at https://pubs.acs.org/doi/10.1021/acssuschemeng.3c00118.

https://doi.org/10.1021/acssuschemeng.3c00118
ACS Sustainable Chem. Eng. 2023, 11, 8035–8043

Table 2. Recent Papers Reporting the Self-Assembly Behavior of CNCs

cellulose source	isolation method	yield (%)	surface charge	phase separation concentration (wt %)	pitch (μm)	reference
degreasing cotton	OA hydrolysis at 105°C for 3 h	24.38	−COOH (0.16 mmol/g)	1.0	4.4 (film)	our work
tunicate	APS oxidation for 16 h followed by ultrasonic treatment for 30min		−COOH (0.40 mmol/g)	3.5	0.302 (film)	He et al.[40]
cotton linter pulp	NaOH treatment for 24 h, H_2SO_4 hydrolysis followed by ionic liquid modification for 24 h		positive electric charge	1	3−4.5	Qin et al.[41]
cotton	organic acid hydrolysis combined with esterification using maleic anhydride and *p*-TsOH as an agent, acetic acid as a solvent	28	−COOH (0.89 mmol/g)	9	2 (film)	Lin et al.[21]
filter paper	molten OA dihydrate heated to 110°C for 15−120 min followed by THF treatment and sonication	71−93	−COOH (0.24−0.54 mmol/g)	chiral nematic order could not be reached		Jia and Liu[42]
softwood dissolving pulp	molten OA dehydrate hydrolysis at 110°C followed by THF treatment and sonication	80.6	−COOH (1.2 mmol/g)	suspension presented birefringence patterns and the film exhibited iridescence		Li et al.[23]
MCC	H_2SO_4 hydrolysis		−SO_3H (0.2 mmol/g)		0.312 (film)	Cheng et al.[43]
	coupled sulfuric acid and acrylic acid treatment		−SO_3H (0.13−0.19 mmol/g), −COOH (0.07−0.11 mmol/g)		0.338−0.409 (film)	
wood pulp, MCC	H_2SO_4 hydrolysis		−SO_3H (0.48−0.52 mmol/g)		0.246−0.350 (film)	Korolovych et al.[44]
cotton pulp	hydrolysis with sulfuric acid coupled with $KMnO_4$ as an oxidizing agent and OA as a reducing agent	48−68	−COOH (0.52−1.58 mmol/g)	7	2.65 (10 wt %)	Zhou et al.[14]
MCC	LPMO enzyme oxidation reaction for 20 h followed by treated with NaOH solution	12.5−13.3	−COOH (0.4−0.7 mmol/g)	3		Koskela et al.[45]
cotton linters	swelling 3 h followed by APS oxidation for 12 h	64.24−95.75	−COOH	observed chiral structure		Wang et al.[46]
cotton	swelling 2 h followed by APS oxidation for 16 h	22−32	−COOH (0.9−2.7 mmol/g)	observed chiral structure		Castro-Guerrero and Gray[47]
cotton linters	H_2SO_4 hydrolysis at 63°C followed by TEMPO-mediated oxidation (TEMPO/NaBr/NaClO, pH = 10−11)		−COOH (0.12 mmol/g)	observed distinct fingerprint texture and birefringence		Azzam et al.[48]

Experimental methods, length and width distribution of CNCs under different conditions, POM image of OA-CNC suspension at a concentration of 6%, AFM images, length and width distribution of ROA-CNCs under different cycles, and POM images of ROA-CNCs under different cycles (PDF)

AUTHOR INFORMATION

Corresponding Authors

Minghua Liu − *College of Environment & Safety Engineering, Fuzhou University, Fuzhou 350108, China; College of Environmental and Biological Engineering, Putian University, Putian 351100 Fujian, China;* orcid.org/0000-0002-5041-790X; Email: mhliu2000@fzu.edu.cn

J. Y. Zhu − *Forest Products Laboratory, U.S. Department of Agriculture, Forest Service, Madison, Wisconsin 53726, United States*; Email: junyong.zhu@usda.gov

Authors

Chunxiang Lin − *College of Environment & Safety Engineering, Fuzhou University, Fuzhou 350108, China;* orcid.org/0000-0003-0506-2537

Ping Wang − *College of Environment & Safety Engineering, Fuzhou University, Fuzhou 350108, China*

Yifan Liu − *College of Environment & Safety Engineering, Fuzhou University, Fuzhou 350108, China*

Yuancai Lv − *College of Environment & Safety Engineering, Fuzhou University, Fuzhou 350108, China*

Xiaoxia Ye − *College of Environment & Safety Engineering, Fuzhou University, Fuzhou 350108, China*

Complete contact information is available at: https://pubs.acs.org/10.1021/acssuschemeng.3c00118

Notes

The authors declare no competing financial interest.

ACKNOWLEDGMENTS

This work was sponsored by the Natural Science Foundation of China (grant no 22208057), Natural Science Foundation of Fujian Province, China (grant no 2020J01506), and on official US government time of Zhu.

REFERENCES

(1) Haouache, S.; Jimenez-Saelices, C.; Cousin, F.; Falourd, X.; Pontoire, B.; Cahier, K.; Jerome, F.; Capron, I. Cellulose nanocrystals from native and mercerized cotton. *Cellulose* **2022**, *29*, 1567−1581.

(2) Habibi, Y.; Lucia, L. A.; Rojas, O. J. Cellulose Nanocrystals: Chemistry, Self-Assembly, and Applications. *Chem. Rev.* **2010**, *110*, 3479−3500.

(3) Giese, M.; Blusch, L. K.; Khan, M. K.; MacLachlan, M. J. Functional materials from cellulose-derived liquid-crystal templates. *Angew. Chem., Int. Ed. Engl.* **2015**, *54*, 2888−2910.

(4) Revol, J.; Godbout, L.; Dong, X.; Gray, D. G.; Chanzy, H.; Maret, G. Chiral nematic suspensions of cellulose crystallites; phase separation and magnetic field orientation. *Liq. Cryst.* **1994**, *16*, 127−134.

(5) Khadem, S. A.; Bagnani, M.; Mezzenga, R.; Rey, A. D. Relaxation dynamics in bio-colloidal cholesteric liquid crystals confined to cylindrical geometry. *Nat. Commun.* **2020**, *11*, 4616−4710.

(6) Zhu, W.; Droguet, B.; Shen, Q.; Zhang, Y.; Parton, T. G.; Shan, X.; Parker, R. M.; De Volder, M. F. L.; Deng, T.; Vignolini, S.; et al. Structurally Colored Radiative Cooling Cellulosic Films. *Adv. Sci.* **2022**, *9*, 2202061.

(7) Kádár, R.; Spirk, S.; Nypelö, T. Cellulose Nanocrystal Liquid Crystal Phases: Progress and Challenges in Characterization Using

Rheology Coupled to Optics, Scattering, and Spectroscopy. *ACS Nano* **2021**, *15*, 7931−7945.
(8) Araki, J.; Kuga, S. Effect of Trace Electrolyte on Liquid Crystal Type of Cellulose Microcrystals. *Langmuir* **2001**, *17*, 4493−4496.
(9) Revol, J.-F.; Bradford, H.; Giasson, J.; Marchessault, R.; Gray, D. Helicoidal self-ordering of cellulose microfibrils in aqueous suspension. *Int. J. Biol. Macromol.* **1992**, *14*, 170−172.
(10) Azzam, F.; Heux, L.; Jean, B. Adjustment of the Chiral Nematic Phase Properties of Cellulose Nanocrystals by Polymer Grafting. *Langmuir* **2016**, *32*, 4305−4312.
(11) Jiao, L.; Bian, H. Y.; Gao, Y.; Lin, X. L.; Zhu, W. Y.; Dai, H. Q. Highly Dispersible Cellulose Nanofibrils Produced via Mechanical Pretreatment and TEMPO-mediated Oxidation. *Fibers Polym.* **2018**, *19*, 2237−2244.
(12) Leung, A. C. W.; Hrapovic, S.; Lam, E.; Liu, Y.; Male, K. B.; Mahmoud, K. A.; Luong, J. H. T. Characteristics and Properties of Carboxylated Cellulose Nanocrystals Prepared from a Novel One-Step Procedure. *Small* **2011**, *7*, 302−305.
(13) Liimatainen, H.; Visanko, M.; Sirvio, J. A.; Hormi, O.; Niinimaki, J. Enhancement of the Nanofibrillation of Wood Cellulose through Sequential Periodate-Chlorite Oxidation. *Biomacromolecules* **2012**, *13*, 1592−1597.
(14) Zhou, L.; Li, N.; Shu, J.; Liu, Y.; Wang, K.; Cui, X.; Yuan, Y.; Ding, B.; Geng, Y.; Wang, Z.; et al. One-Pot Preparation of Carboxylated Cellulose Nanocrystals and Their Liquid Crystalline Behaviors. *ACS Sustainable Chem. Eng.* **2018**, *6*, 12403−12410.
(15) Yu, H.; Chen, G.; Wang, Y.; Yao, J. A facile one-pot route for preparing cellulose nanocrystal/zinc oxide nanohybrids with high antibacterial and photocatalytic activity. *Cellulose* **2015**, *22*, 261−273.
(16) Liu, P.; Pang, B.; Dechert, S.; Zhang, X. C.; Andreas, L. B.; Fischer, S.; Meyer, F.; Zhang, K. Structure Selectivity of Alkaline Periodate Oxidation on Lignocellulose for Facile Isolation of Cellulose Nanocrystals. *Angew. Chem., Int. Ed.* **2020**, *132*, 3244−3251.
(17) Nyström, G.; Arcari, M.; Adamcik, J.; Usov, I.; Mezzenga, R. Nanocellulose Fragmentation Mechanisms and Inversion of Chirality from the Single Particle to the Cholesteric Phase. *ACS Nano* **2018**, *12*, 5141−5148.
(18) Bian, H.; Chen, L.; Gleisner, R.; Dai, H.; Zhu, J. Y. Producing wood-based nanomaterials by rapid fractionation of wood at 80 °C using a recyclable acid hydrotrope. *Green Chem.* **2017**, *19*, 3370−3379.
(19) Chen, L.; Zhu, J. Y.; Baez, C.; Kitin, P.; Elder, T. Highly thermal-stable and functional cellulose nanocrystals and nanofibrils produced using fully recyclable organic acids. *Green Chem.* **2016**, *18*, 3835−3843.
(20) Wang, R.; Chen, L.; Zhu, J.; Yang, R. Tailored and Integrated Production of Carboxylated Cellulose Nanocrystals (CNC) with Nanofibrils (CNF) through Maleic Acid Hydrolysis. *ChemNanoMat* **2017**, *3*, 328−335.
(21) Lin, C.; Chen, B.; Liu, Y.; Chen, Y.; Liu, M.; Zhu, J. Y. Carboxylated cellulose nanocrystals with chiral nematic property from cotton by dicarboxylic acid hydrolysis. *Carbohydr. Polym.* **2021**, *264*, 118039.
(22) Jia, C.; Chen, L.; Shao, Z.; Agarwal, U. P.; Hu, L.; Zhu, J. Y. Using a fully recyclable dicarboxylic acid for producing dispersible and thermally stable cellulose nanomaterials from different cellulosic sources. *Cellulose* **2017**, *24*, 2483−2498.
(23) Li, D.; Henschen, J.; Ek, M. Esterification and hydrolysis of cellulose using oxalic acid dihydrate in a solvent-free reaction suitable for preparation of surface-functionalised cellulose nanocrystals with high yield. *Green Chem.* **2017**, *19*, 5564−5567.
(24) Kelly, J. A.; Shukaliak, A. M.; Cheung, C. C. Y.; Shopsowitz, K. E.; Hamad, W. Y.; MacLachlan, M. J. Responsive Photonic Hydrogels Based on Nanocrystalline Cellulose. *Angew. Chem., Int. Ed.* **2013**, *52*, 8912−8916.
(25) Segal, L.; Creely, J.; Martin, A.; Conrad, C. An empirical method for estimating the degree of crystallinity of native cellulose using the X-ray diffractometer. *Text. Res. J.* **1959**, *29*, 786−794.
(26) Elazzouzi-Hafraoui, S.; Nishiyama, Y.; Putaux, J.; Heux, L.; Dubreuil, F.; Rochas, C. The Shape and Size Distribution of Crystalline Nanoparticles Prepared by Acid Hydrolysis of Native Cellulose. *Biomacromolecules* **2008**, *9*, 57−65.
(27) Sun, B.; Zhang, M.; Hou, Q. X.; Liu, R.; Wu, T.; Si, C. L. Further characterization of cellulose nanocrystal (CNC) preparation from sulfuric acid hydrolysis of cotton fibers. *Cellulose* **2016**, *23*, 439−450.
(28) Gray, D. G. The surface analysis of paper and wood fibers by ESCA. III. Interpretation of carbon (1s) peak shape. *Cellul. Chem. Technol.* **1978**, *6*, 735−743.
(29) Wang, Y. X.; Lwal, A.; Wang, Q.; Zhou, J.; Dufresne, A.; Lin, N. Regulating surface sulfonation on cellulose nanocrystals and self-assembly behaviors. *Chem. Commun.* **2020**, *56*, 10958−10961.
(30) Lu, T.; Pan, H.; Ma, J.; Li, Y.; Bokhari, S. W.; Jiang, X.; Zhu, S.; Zhang, D. Cellulose Nanocrystals/Polyacrylamide Composites of High Sensitivity and Cycling Performance To Gauge Humidity. *ACS Appl. Mater. Interfaces* **2017**, *9*, 18231−18237.
(31) Wu, Q.; Meng, Y.; Wang, S.; Li, Y.; Fu, S.; Ma, L.; Harper, D. Rheological behavior of cellulose nanocrystal suspension: Influence of concentration and aspect ratio. *J. Appl. Polym. Sci.* **2014**, *131*, 40525.
(32) Raghuwanshi, V. S.; Browne, C.; Batchelor, W.; Garnier, G. Self-assembly of cellulose nanocrystals of different lengths. *J. Colloid Interface Sci.* **2023**, *630*, 249−259.
(33) Beck-Candanedo, S.; Roman, M.; Gray, D. G. Effect of Reaction Conditions on the Properties and Behavior of Wood Cellulose Nanocrystal Suspensions. *Biomacromolecules* **2005**, *6*, 1048−1054.
(34) Vroege, G. J.; Lekkerkerker, H. N. W. Theory of the Isotropic-Nematic-Nematic Phase Separation for a Solution of Bidisperse Rodlike. *J. Phys. Chem.* **1993**, *14*, 3601−3605.
(35) Mu, X.; Gray, D. G. Formation of Chiral Nematic Films from Cellulose Nanocrystal Suspensions Is a Two-Stage Process. *Langmuir* **2014**, *30*, 9256−9260.
(36) Lagerwall, J.; Schutz, C.; Salajkova, M.; Noh, J.; Hyun Park, J.; Scalia, G.; Bergstrom, L. Cellulose nanocrystal-based materials: from liquid crystal self-assembly and glass formation to multifunctional thin films. *NPG Asia Mater.* **2014**, *6*, No. e80.
(37) Casado, U.; Mucci, V.; Aranguren, M. I. Cellulose nanocrystals suspensions: Liquid crystal anisotropy, rheology and films iridescence. *Carbohydr. Polym.* **2021**, *261*, 117848−117914.
(38) Chen, H.; Hou, A.; Zheng, C.; Tang, J.; Xie, K.; Gao, A. Light- and Humidity-Responsive Chiral Nematic Photonic Crystal Films Based on Cellulose Nanocrystals. *ACS Appl. Mater. Interfaces* **2020**, *12*, 24505−24511.
(39) Zheng, H. Z.; Li, W. R.; Li, W.; Wang, X. J.; Tang, Z. Y.; Zhang, S.; Xu, Y. Uncovering the Circular Polarization Potential of Chiral Photonic Cellulose Films for Photonic Applications. *Adv. Mater.* **2018**, *30*, 1705948.
(40) He, J.; Bian, K.; Piao, G. Self-assembly properties of carboxylated tunicate cellulose nanocrystals prepared by ammonium persulfate oxidation and subsequent ultrasonication. *Carbohydr. Polym.* **2020**, *249*, 116835.
(41) Qin, J. L.; Wang, Z. L.; Hu, J.; Yuan, Y.; Liu, P.; Cheng, L.; Kong, Z. Q.; Liu, K.; Yan, S. K.; Zhang, J. M. Distinct liquid crystal self-assembly behavior of cellulose nanocrystals functionalized with ionic liquids. *Colloids Surf., A* **2022**, *632*, 127790.
(42) Jia, W.; Liu, Y. Two characteristic cellulose nanocrystals (CNCs) obtained from oxalic acid and sulfuric acid processing. *Cellulose* **2019**, *26*, 8351−8365.
(43) Cheng, Z.; Ye, H. L.; Cheng, F.; Li, H. Y.; Ma, Y.; Zhang, Q.; Natan, A.; Mukhopadhyay, A.; Jiao, Y. C.; Li, Y.; et al. Tuning Chiral Nematic Pitch of Bioresourced Photonic Films via Coupling Organic Acid Hydrolysis. *Adv. Mater. Interfaces* **2019**, *6*, 1802010.
(44) Korolovych, V. F.; Cherpak, V.; Nepal, D.; Ng, A.; Shaikh, N. R.; Grant, A.; Xiong, R.; Bunning, T. J.; Tsukruk, V. V. Cellulose nanocrystals with different morphologies and chiral properties. *Polymer* **2018**, *145*, 334−347.

https://doi.org/10.1021/acssuschemeng.3c00118
ACS Sustainable Chem. Eng. 2023, 11, 8035−8043

(45) Koskela, S.; Wang, S. N.; Fowler, P.; Tan, F. C.; Zhou, Q. Structure and Self-Assembly of Lytic Polysaccharide Monooxygenase-Oxidized Cellulose Nanocrystals. *ACS Sustainable Chem. Eng.* **2021**, *9*, 11331−11341.
(46) Wang, H.; Pudukudy, M.; Ni, Y. H.; Zhi, Y. F.; Zhang, H.; Wang, Z. Q.; Jia, Q. M.; Shan, S. Y. Synthesis of nanocrystalline cellulose via ammonium persulfate-assisted swelling followed by oxidation and their chiral self-assembly. *Cellulose* **2020**, *27*, 657−676.
(47) Castro-Guerrero, C. F.; Gray, D. G. Chiral nematic phase formation by aqueous suspensions of cellulose nanocrystals prepared by oxidation with ammonium persulfate. *Cellulose* **2014**, *21*, 2567−2577.
(48) Azzam, F.; Heux, L.; Jean, B. Adjustment of the Chiral Nematic Phase Properties of Cellulose Nanocrystals by Polymer Grafting. *Langmuir* **2016**, *32*, 4305−4312.

https://doi.org/10.1021/acssuschemeng.3c00118
ACS Sustainable Chem. Eng. 2023, 11, 8035−8043